Biomaterials Science

Self-assembling peptides cross-linked with Genipin: resilient hydrogels and self-standing electrospun scaffolds for tissue engineering applications

Journal:	*Biomaterials Science*
Manuscript ID	BM-ART-07-2018-000825.R1
Article Type:	Paper
Date Submitted by the Author:	30-Oct-2018
Complete List of Authors:	Pugliese, Raffaele; A.O.Niguarda Ca'Granda, Center for Nanomedicine and Tissue Engineering Maleki, Mahboubeh; Ospedale Casa Sollievo della Sofferenza, ISBREMIT; Ospedale Niguarda, Center for Nanomedicine and Tissue Engineering Zuckermann, Ronald; The Molecular Foundry, Biological Nanostructures Facility Gelain, Fabrizio; A.O.Niguarda Ca'Granda, Center for Nanomedicine and Tissue Engineering

Journal Name

ARTICLE

Self-assembling peptides cross-linked with Genipin: resilient hydrogels and self-standing electrospun scaffolds for tissue engineering applications

Received 00th January 20xx,
Accepted 00th January 20xx

DOI: 10.1039/x0xx00000x

www.rsc.org/

Raffaele Pugliese[a,b], Mahboubeh Maleki[a], Ronald N. Zuckermann[c] and Fabrizio Gelain[a,b,*]

Self-assembling peptides (SAPs) are synthetic bioinspired biomaterials that can be feasibly multi-functionalized for applications in surgery, drug delivery, optics and tissue engineering (TE). Despite their promising biocompatibility and biomimetic properties, they have never been considered real competitors of polymers and/or cross-linked extracellular matrix (ECM) natural proteins. Indeed, synthetic SAP-made hydrogels usually feature modest mechanical properties, limiting their potential applications, due to the transient non-covalent interactions involved in the self-assembling phenomenon. Cross-linked SAP-hydrogels have been recently introduced to bridge this gap, but several questions remain open. New strategies leading to stiffer gels of SAPs may allow for a full exploitation of the SAP technology in TE and beyond. We have developed and characterized a genipin cross-linking strategy significantly increasing stiffness and resiliency of FAQ(LDLK)$_3$, a functionalized SAP already used for nervous cells cultures. We characterized different protocols of cross-linking, analyzing their dose and time-dependent efficiency, influencing stiffness, bioabsorption time and molecular arrangements. We choose the best developed protocol to electrospun into nanofibers, first time ever, self-standing, water-stable and flexible fibrous mats and micro-channels entirely made of SAPs. This work may open the door to the development and tailoring of bioprostheses entirely made of SAPs for different TE applications.

Keywords: cross-linking; self-assembling peptide; genipin; rheology; electrospinning; micro-channel

Introduction

The field of self-assembling peptides (SAPs) has undergone an outstanding growth since early 1990s, when Shuguang Zhang serendipitously discovered a segment of a yeast protein capable of self-assembling.[1] Since then, self-assembling peptides have been used as hemostat solutions,[2-4] nanocarriers of drugs,[5-8] bone fillers,[9-11] wound healers,[12-14] but also as injectable scaffolds for the regeneration of injured heart,[15-17] cartilage and[18, 19] nucleus pulposus.[20, 21] The field of peptide scaffolds is still expanding at an accelerating pace, and a few clinical trials are currently assessing their potential for remineralization in dental repair [22, 23] and their sealing properties in post-operative lymphorrhea following pelvic surgery.[24]

SAPs are made of amino acids and self-assemble into various nanostructures (nanofibers, nanotubes and nanovesicles) upon exposure to shifts of pH, temperature and osmolarity. These structures can mimic the natural peptide-based extracellular matrix (ECM), and can also display multiple, specific functional motifs capable of interacting with cells[25, 26] and proteins[27, 28] (if designed to do so). Furthermore, SAPs are synthetic, pathogen-free, biodegradable and mainly used at low concentrations in water (less than 8%, w/v), all desirable properties for translational therapies in the future.

Despite their extensive use in different areas of material science and regenerative medicine, several applications of SAPs are still precluded because of their poor mechanical stability, mainly arising from the non-covalent interactions within supramolecular assemblies.[29] As a matter of fact, most of the SAP-based therapies focused their efforts on the biochemical composition of the target tissue to be regenerated, while biomechanical properties were still out-of-reach. Indeed, scaffold biomechanical properties should be reliably tuned in order to presumably match those of the target tissue and to expand their potential range of applications. In addition, the improvement of both architectural (e.g. nano-topography) and mechanical (e.g. elasticity and stiffness) features could make these materials tailorable via electrospinning (ES), a nano- and micro-fabrication versatile technique widely used in TE,[30-32] but rarely used with SAPs because of their intrinsic limited molecular weight and viscoelastic properties. So far, electrospun SAP fibers have been produced in biopolymer blends or alone as coatings.[33, 34]

We recently demonstrated how cross-linking could be a viable strategy to fill some of these goals:[35] however, the biocompatibility

[a] IRCSS Casa Sollievo della Sofferenza, Unità di Ingegneria Tissutale, Viale Cappuccini 1, San Giovanni Rotondo (FG) 71013, Italy
[b] Center for Nanomedicine and Tissue Engineering (CNTE), ASST Grande Ospedale Metropolitano Niguarda, Piazza dell'Ospedale Maggiore 3, Milan 20162, Italy
[c] The Molecular Foundry, Lawrence Berkeley National Laboratory, 1 Cyclotron road, Berkeley, California 94720, United States
* Corresponding Author: f.gelain@css-mendel.it (F. Gelain)
Electronic Supplementary Information (ESI) available: [Biomechanics assessment of different cross-linking SAPs; AFM morphological analysis; *In vitro* degradation of cross-linked hydrogels; QC of electrospun cross-linked nanofibrous scaffolds]. See DOI: 10.1039/x0xx00000x

of the cross-linking agent we used (i.e. sulfo-SMCC) as well as the specific SAP sequence requirements (comprising both cysteine and lysine residues) may pose some limitations in the future.

Genipin, extracted from *Gardenia jasminoides Ellis* fruits, is a naturally occurring cross-linking agent used in Chinese medicine[36, 37] that specifically reacts with primary amines of peptides and proteins. To date, it has been employed for the cross-linking of gelatin,[38-40] chitosan[41, 42] and Fmoc-triphenyalanine hydrogel[43] with far less cytotoxicity (5,000-10,000 times) than glutaraldehyde. It was demonstrated to reverse clinical symptoms of diabetes[44] and to exert anti-inflammatory,[45-48] anti-oxidative,[49] neuroprotective (in Alzheimer's diseases), [50, 51] and anti-cancer effects in colorectal[52, 53], breast[54], and prostate[55] cancers, as well as pancreatic adeno- [56], hepato- [57, 58] and gastric carcinomas.[59-61]

We here introduced and optimized a genipin (gp) cross-linking reaction to stabilize biomimetic hydrogels made of FAQ$(LDLK)_3$ (i.e. NH_2-FAQRVPPGGGLDLKLDLKLDLK-$CONH_2$) SAP. By using genipin, we significantly increased stiffness and failure stress of FAQ$(LDLK)_3$, both increments dependent on dose and exposure-time to the cross-linking agent. While still preserving SAP secondary structure arrangements, stress-relaxation properties of the hydrogels were modulated by using different genipin concentrations and delivery strategies. These enhancements allowed us to electrospun cross-linked SAPs to obtain, for the first time, water-stable (but bioabsorbable), self-standing and flexible nano- and micro-fibrous mats and micro-channels entirely made of functionalized SAPs. Literally this work will open the door of SAPs to the field of electrospun scaffolds, yielding to biomimetic synthetic bioprostheses with tunable resilience, bioabsorption times and/or bioactivities, for several TE applications like heart patches, skin dressing, blood vessel implants and so on.

Experiment

Peptide synthesis and purification

Peptides were synthesized using fluorenylmethoxycarbonyl (Fmoc) solid-phase peptide synthesis with the Liberty-Discovery (CEM) microwave automated synthesizer and were purified as previously described. [26] Briefly, synthesis was carried out with 0.5M HBTU in DMF and 2M DIEA in NMP as activator and activator base solutions respectively. Peptide was synthesized by using a rink-amide resin (0.5 mmol/g). Fmoc-protected amino acids were dissolved at 0.2M in DMF, the deprotection solution for Fmoc-group removal was 20% (v/v) 4-metylpiperidin in DMF. Removal of side-chain protecting groups and cleavage was obtained with TFA:TIS:H_2O (95:2.5:2.5) cocktail. A three-glycine spacer, interposed between the FAQRVPP functional motif [26] and the $(LDLK)_3$ self-assembling backbone constitute the FAQ$(LDLK)_3$ peptide. Raw peptide was precipitated using cold ethyl ether and then lyophilized (Labconco). The resulting raw peptide was purified using a Waters binary high-performance liquid chromatography (HPLC) apparatus (>95%). The molecular weight of purified peptide has been identified via single quadrupole mass detection (Waters LC-MS Alliance-3100). Purified peptide powder was subsequently dissolved in 0.1M HCl solution in order to remove the presence of possible TFA salts.

Cross-linked SAP hydrogel preparation

Diffusive cross-linking reaction (DCR). The purified peptide was dissolved at a concentration of 5% (w/v) in distilled water, sonicated for 30min and incubated at 4°C for 24h, the day prior to the cross-linking reaction. Right before the cross-linking reaction genipin powder (Sigma Aldrich) was dissolved in 100µl of PBS (Thermofisher scientific 1X, w/o $MgCl_2$ and $CaCl_2$) and EtOH (95:5 v/v; pH=7.4) and filtered (0.22µm pore size). Genipin cross-linked hydrogels were prepared by adding 86mM and 170mM of genipin to 50µl of peptide (5% w/v) and incubated at 37°C for 72h. At the end of the reaction, the unreacted genipin in the supernatant was removed by aspiration with a vacuum pipette, and the resulting cross-linked hydrogel was washed and suspended in 1.5 ml of PBS for 1h. Washes were repeated 5 times before use.

In situ cross-linking reaction (ISCR). *In situ* genipin cross-linked hydrogel was prepared by adding 86mM and 170mM of genipin dissolved in 100µl of H_2O:PBS:EtOH (47.5:47.5:5 v/v) to the purified peptide powder to achieve a final 5% (w/v) concentration.. The mixed solution was sonicated for 30min and incubated at 37°C for 72h.

In situ partial cross-linking reaction (ISPCR). *In situ* partial cross-linked hydrogel was prepared by adding 14.6mM and 29.6mM of genipin dissolved in 100µl of H_2O:EtOH (95:5 v/v) to the purified peptide powder to achieve a final 1% (w/v) concentration. The mixed solutions were then sonicated for 30min and incubated at 37°C for 24h. See Table S1 in the ESM for all abbreviations used in the manuscript.

All experiments were performed over a wide range of concentrations and treatment times to assess genipin-dosing regimens influencing SAP-hydrogels mechanical properties.

Electrospinning of cross-linked SAP scaffolds

Electrospun nanofibers (es-FAQ$(LDLK)_3$/gp) were fabricated using *In situ partial cross-linked* FAQ$(LDLK)_3$/gp (14.6mM, 72h) by a single-jet customized electrospinning system. The spinning solvent to dissolve the FAQ$(LDLK)_3$/gp (14.6mM, 72h) was 1,1,1,3,3,3-hexafluoro-2-propanol (HFIP, Sigma Aldrich). ES solution was sonicated for 30 min, and after 1h rest it was employed for ES. All sample preparations were carried out under ambient conditions. The peptide solution at 35% (w/v) in 100% HFIP was placed in a syringe with a 29-gauge needle (1 ml BD™ U-100 insulin syringe) mounted on a syringe pump (NewEra NE-1000). The syringe pump was used to provide a constant stream of solution at the tip of the needle. The electrical potential of 12-15 kV was applied to the needle by a power supply (Spellman High Voltage, 0-30 kV). A 33G micro-needle (Hamilton needle, stainless steel, outer diameter =210 µm, length 51 mm) as collector was fixed to a rotating arm of a non-conductive mandrel (length 12 cm, ≈40 rpm) and grounding electrode was indirectly (using a copper ring) placed at the end of micro-needle in order to provide a constant speed for a uniform fiber collection around micro-needle. Spinning was performed under ambient conditions (23-25 °C) with a humidity range of 35-40%. A seamless micro-conduit of es-FAQ$(LDLK)_3$/gp was obtained when the selected micro-channel was post-treated (PT). The optimized procedure involved exposure to vapor phase of NaOH 2.5mM in PBS (PT-I) for 3 days to slightly activate the genipin while stabilizing the fibers morphological stability, followed by 1 day immersion of 170mM genipin in H_2O:EtOH (90:10 v/v) (PT-II). Subsequently, the cross-linking process was terminated by soaking the micro-channel in PBS for 1 day (PT-III) to remove any trace amounts of used ethanol. All the PT phases were done at 37°C under 95% O_2/5% CO_2 atmosphere (Caron's Oasis™ CO_2/O_2 Incubator, Marietta, OH, USA).

Rheological tests

Rheological properties of assembled nanostructures were investigated with a controlled stress AR-2000ex Rheometer (TA instruments). A truncated cone-plate geometry (acrylic truncated diameter, 20 mm; angle, 1°; truncation gap, 34 μm) was used. All measurements were done at 25°C (Peltier cell) and all samples were tested one day after dissolution at 1% and 5% (w/v) concentrations. To monitor the sol-gel transition and to evaluate the storage (G') and loss (G") moduli increase as a function of time, a time-sweep test at constant angular frequency (ω= 1Hz) was carried out for 15h. For FAQ(LDLK)$_3$ (without genipin) the assembly was triggered by adding PBS laterally to the peptide solution positioned in the 34μm cone-plate truncation gap, while for the genipin cross-linked peptides (FAQ(LDLK)$_3$/gp) both assembly and cross-linking were triggered by adding genipin in PBS:EtOH (95:5 v/v). Afterwards, in the linear viscoelastic region, a frequency sweep test (0.1-1,000 Hz, 1% strain) was performed to measure G' and G" of the scaffolds. Stress/strain sweeps were performed (0.01%-1000%) to identify the limits of the linear viscoelastic region and the maximum strain and stress to which the sample can be subjected. On the assembled genipin cross-linked hydrogels (0.5cm in diameter, 2mm thick, equilibrated in PBS for 24h), stress-relaxation tests were performed at 10% strain held constant and with a deformation rate of 1mm min^{-1}. Load was recorded as a function of time. Stress-relaxation data and $\tau_{½}$ (time for the initial stress of material to halve throughout the test) were evaluated using a two-element Maxwell-Weichert linear viscoelastic model.[62] Lastly, a temperature ramp was recorded as a function of G' (T_{rate}= 5°C/min, 1% strain, ω= 1Hz). Each experiment was performed in triplicate.

2,4,6-trinitrobenzene sulfonic acid (TNBSA) assay

The cross-linking degree of FAQ(LDLK)$_3$/gp was assessed using TNBSA (Thermo Scientific), which specifically reacts with primary amine groups in peptides/proteins, yielding to a yellow-colored product that can be monitored at 335nm. Primary amine groups are quantified based on molar absorptivity using the extinction coefficient of TNBSA (10,000 M^{-1} cm^{-1}). [63] 100μl of peptides were treated with TNBSA (50μl, 0.01% w/v in 0.1 M $NaHCO_3$, pH=8.5) and incubated for 2h at 37°C. To stop the reaction 25μl of 1N HCl was added to the solution. Measurements were performed via a 1cm spectrophotometric cuvette using an Infinite M200 Pro plate reader (Tecan). For each sample, primary amine groups were estimated at 0, 2, 4, 6, 8, 24, 32, 48, 72 and 120 hours. 0.1M $NaHCO_3$ was used as blank. [64] All measurements were processed with Origin™8 software using Logistic fitting.

Fluorescence measurements

The effect of the formation of blue pigmentation that qualitatively indicates genipin cross-linking [65] was measured through the fluorescence intensity as a function of cross-linking time. The FAQ(LDLK)$_3$ peptide was used as control. Genipin fluorescence intensity was recorded using an Infinite M200 PRO plate reader (Tecan) with λ_{ex}= 590nm and λ_{em}= 630nm, from 0h to 120h at 25°C. All experimental runs were repeated three times per each different timepoint. Background fluorescence was subtracted from each spectrum. Lastly, spectra were averaged and processed with Origin™8 software using Boltzmann fitting.

Fourier transforms infrared spectroscopy (FTIR) analysis

FTIR analysis of assembled nanostructures was performed on FAQ(LDLK)$_3$ dissolved at a concentration of 1% and 5% (w/v) in distilled water, and on DCR, ISCR and ISPCR peptides after a 24h-incubation at 4°C. All spectra were recorded in attenuated total reflection (ATR) using Perkin Elmer Spectrum 100 spectrometer. A 2μl aliquot of the FAQ(LDLK)$_3$ peptide solution and of the DCR, ISCR and ISPCR films were deposited on the reflection diamond element and let to evaporate. Twenty acquisitions were recorded for each spectrum, using the following conditions: 4cm^{-1} spectrum resolution, 25kHz scan speed, 1000 scan co-addition and triangular apodization. All the collected spectra were reported after ATR correction, smoothing and automatic baseline correction using Origin™8 software. Each sample preparation was repeated three times.

X-ray diffraction (XRD) analysis

XRD patterns were collected using a multiple-wavelength anomalous diffraction and monochromatic macromolecular crystallography beamline (8.3.1) located at the Advanced Light Source (ALS), Lawrence Berkeley National Laboratory, as previously described. [35, 66] All samples were prepared 24h before the analysis and stored at 4°C. On the day of the analysis FAQ(LDLK)$_3$ peptide solution at the concentration of 1% and 5% (w/v) was centrifuged at 12,000rpm for 10min and the resulting concentrated pellet was dropped on MicroRT™ X-ray Capillary (Mitegen) and let to evaporate. Genipin cross-linked peptides were placed directly on MicroRT™ X-ray Capillary and let to evaporate. Data were analyzed with FIT2D [67] and processed with Origin™8 software.

Atomic force microscopy (AFM) analysis

AFM images were captured in tapping mode by a Multimode Nanoscope V (Digital Instrument, Veeco), using a single-beam silicon cantilever probes (Veeco RFESP MPP-21100-10, cantilever f0, resonance frequency 59-69 KHz, constant force 3 N m^{-1}). FAQ(LDLK)$_3$ peptide was dissolved in distilled water the day prior to imaging, whereas DCR and ISCR peptides were measured at 32h of cross-linking reaction time. Right before the analysis, peptides solutions were diluted to a final concentration of 0.001% (w/v) and deposited on a freshly cleaved mica surface. A 2μl of each solution was kept on the mica for 4 min at RT, subsequently rinsed with distilled water (to remove loosely bound peptides), and dried at RT for 30min, thus ready for imaging. 100 different nanofibers of approximately 10 independent fields per sample were measure and characterized as previously described. [68]

Scanning electron microscopy (SEM) analysis

Electrospun fibers from mats and microchannels were analyzed with the aid of scanning electron microscopy (SEM; Tescan Vega) after sputter coated with ≈12 nm of Au (Quorum Q150R S), as previously described. [34]

The average and standard deviation of the electrospun fiber diameters were measured by choosing 100 fibers and analyzing them using IMAGEJ software (v.1.45s, National Institute of Health, USA).

Trypsin degradation *in vitro*

The degradation of genipin cross-linked peptides was investigated by monitoring the scaffold weight loss upon trypsin exposure (10mg/ml PBS, pH=7.4, Sigma Aldrich) at 37°C. [69] In brief, DCR (100µl, 5% w/v) and ISPCR (100µl, 1% w/v) peptides were immersed in trypsin solution (2ml, pH 7.4) and incubated at 37°C. Enzyme solution was changed every week. At given time points, the cross-linked peptides were taken out, washed and lyophilized. The degradation ratio was calculated by comparing the weight loss of the scaffolds with the initial dry weight using the following equation:

$$\text{Degradation (\%)} = [(W_0 - W_t)/W_0] \times 100$$

where W_0 is the initial dry weight of the scaffold, and W_t is the dry weight of the scaffold at a given time point. In addition, the supernatant of each sample was taken out to evaluate the presence of hydrolyzed/degraded peptide and the release of genipin by monitoring absorbance and fluorescence respectively.

Cell Morphology, Viability and Differentiation Assays

Human Neural Stem Cells (hNSCs) were obtained according to good manufacturing practice protocols (GMP) in agreement with the guidelines of European Medicines Agency (EMA) and Agenzia Italiana del Farmaco (AIFA).[70] hNSCs were expanded as previously described.[71] Briefly, hNSCs were cultured to a neurosphere state and mechanically dissociated. The day after, cells were seeded on the surface of FAQ(LDLK)$_3$ hydrogel (3 x 10^4 cells/cm^2), exposed to different concentrations of genipin and cultured for 1 day in vitro (1DIV). Cultrex-BME substrate (R&D systems; 150 µg mL^{-1} in basal medium) was used as a positive control substrate. Cell viability was assessed using commercially available LIVE/DEAD cell viability assay kit (Thermofisher scientific). hNSC were differentiated in standard differentiation medium on top of es-FAQ(LDLK)$_3$/gp mats and immunostained at 7DIV. Further details are provided in the Electronic Supplementary Material (ESM).

Statistical analysis

Data were processed using GraphPad Prism 7 software. Rheological tests were assessed by one-way ANOVA followed by Tukey's multi-comparison test. p<0.05 was considered statistically significant.

Results and Discussion

Design and fabrication of cross-linked functionalized-SAP hydrogels

LDLK12 peptides containing alternating charged hydrophilic and hydrophobic amino acid residues have strong propensity to cross-β-sheet formation at physiological conditions of pH and temperature; also, hydrophobic forces, electrostatic and VDW interactions drive their assembly into nanofibers featuring charged hydrophilic and hydrophobic residues respectively exposed to the aqueous environment and packed in a hydrophobic inner pocket. [29, 72] These designer SAPs can be feasibly functionalized with functional motifs at C- or -N terminal to obtain biomimetic scaffolds customized for specific applications. [26, 73, 74] Usually, functional motifs are short peptides (2-16 amino acids) linked to the self-assembling backbone through a spacer (comprising a few glycines) to ensure flexibility and exposure to target binding.[75] Also, multiple different functionalizations can be included with ease within the same scaffold in order to merge different TE strategies within the same implant (e.g. cell transplants, drug delivery, *in vivo* tracking, etc).

We previously demonstrated that upon exposure to neutral-pH solutions, the designer FAQRVPP-LDLK12 functionalized sequence self-assembles into nanofibers flanked by the added motifs [26], providing functionalized microenvironments with specific biological cues capable of stimulating adult neural stem cell (NSC) adhesion and differentiation. Indeed, the phage display-derived FAQRVPP motif enhanced both neuronal and oligodendroglial differentiation of mNSCs and hNSCs in *in vitro* 2D cultures and favored nervous regeneration in acute spinal cord injuries (SCI) in rats without altering the physiological inflammatory response following the initial insult. [26] However, FAQRVPP-LDLK12 spontaneously forms weak and fragile hydrogel scaffolds with limited flexibility and processing potential, i.e. suitable mainly for the regeneration of soft tissues or as fillers. Conversely, by applying a genipin cross-linking reaction to stabilize the primary-amines of FAQRVPP-LDLK12 (described in Experiment, section Cross-linked SAP hydrogel preparation**)** we obtained scaffolds made of cross-linked functionalized SAPs displaying remarkable improvements in resilience, stress-relaxation and processability. Thus, by using *In situ cross-linking reaction* (ISCR), we managed to cross-link functionalized hydrogels with tunable mechanical properties (Fig. 1a) suitable for TE applications precluded so far. *Vice versa*, by using *Diffusive cross-linking reaction* (DCR), we obtained hollow microchannels (Fig. 1b) and flexible membranes resilient to compression (Fig. 1c and Video S1 in the ESM). Furthermore, as genipin mainly interacts with the Lysine-rich backbone sequence, different functionalizations [68, 76] can be added to the same self-assembling backbone and mixed prior to self-assembling in order to have multi-functionalized scaffolds for multi-target therapies.

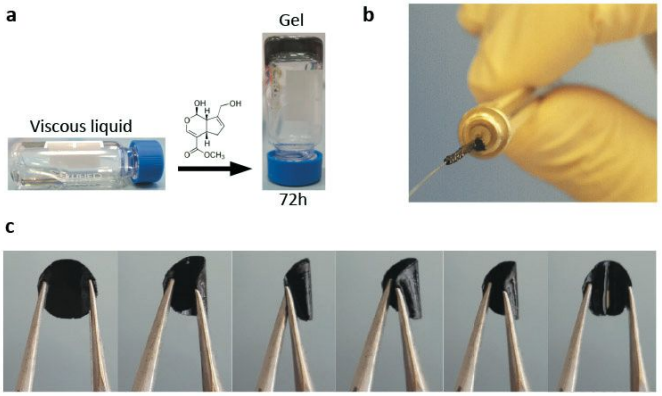

Figure 1. Examples of SAP cross-linked scaffolds: (a) ISCR-FAQ(LDLK)$_3$/gp functionalized hydrogel with tunable mechanical properties after 72h of reaction; (b) hollow flexible microchannel obtained via DCR; (c) flexible DCR-FAQ(LDLK)$_3$/gp membrane resilient to compression.

Biomechanical characterization

SAP-hydrogels are materials of choice in diverse applications (i.e. scaffolds for regenerative medicine,[2, 29, 71, 77-79] carriers for drug delivery, [80-82] actuators for optics and fluidics [83], and ECM models for biological studies [84]), but their usage is often limited by their

poor mechanical properties. Indeed, most SAPs are brittle and do not exhibit enough stretchability. Accordingly, it was crucial to assess how the differently genipin cross-linking strategies influenced their mechanical strength, thus enlarging their range of potential applications. In the case of hydrogels the most relevant biomechanical features to be characterized are the storage (G') and loss (G") moduli. The former reflects the stiffness trend of the biomaterial, and its increase as a function of time can be indicative of over-structural kinetic and networking processes of the sample, while the latter represents the energy dissipated during the test and correlates with the liquid-like response of the hydrogel. The ratio between G' and G" provides insights of the viscoelastic profile of tested material, i.e. whether it behaves as a viscous liquid (G'<G") or as an elastic solid (G'>G"). [85] We investigated two different protocols for the cross-linking reaction, DCR and ISCR (see Experiment for details), in order to elucidate differences, if any, arising by two ways of administration of genipin to the functionalized SAP. Indeed DCR could be seen interesting for post-assembling treatments of a preformed scaffold while ISCR may look similar to an injectable self-polymerizing agent.

By monitoring the temporal evolution of G' and G", the increasing hydrogel stiffness was observed for FAQ(LDLK)$_3$/gp peptides using DCR (Fig. 2a), ISCR (Fig. 2b) and for the un-cross-linked FAQ(LDLK)$_3$ peptide (Fig. 2a). The latter reached a plateau after 5h, displaying an average G' value of 0.7 kPa, which is typical of soft SAP hydrogels and in agreement with our previously published results. [25] By contrast, the storage modulus of genipin cross-linked peptides increased linearly as a function of the reaction-time, reaching a plateau after ≈11h. Close to the equilibrium, the average G' profile of DCR-FAQ(LDLK)$_3$/gp (86mM) and DCR-FAQ(LDLK)$_3$/gp (170mM) was 72 kPa and 110 kPa respectively. While for the ISCR-FAQ(LDLK)$_3$/gp (86mM) and ISCR-FAQ(LDLK)$_3$/gp (170mM) the average G' value is shifted respectively to 39.5 kPa and 70 kPa. This increase in the storage modulus was likely due to the formation of covalent cross-links concomitant with self-assembly, both activated by the shift of pH and temperature. Self-assembly is usually a fast process (SAPs macroscopic hydrogelation can be a matter of a few seconds), while genipin cross-linking could be much slower (from 24h to 72h). Hence, the difference of stiffness between the FAQ(LDLK)$_3$/gp peptides with DCR and ISCR (at same genipin concentration) can be attributed to the fact that in DCR, where samples feature pre-assembled β-rich structures, the interactions among genipin and the already self-assembled fibers lead to the formation of an efficiently entangled nanofibrous network with increased values of G'. We hypothesize that in the case of ISCR, genipin is presumably uniformly distributed throughout the sample before self-assembly and the two phenomena are concomitant (even if for a short period of time) after pH-shift (see Experiment for details): this may have influenced the stabilization of the forming β-sheet domains and consequently the mechanical strength of the hydrogel. This consideration will be better investigated in the next sections, but, in our opinion, will need a mandatory confirmation through hybrid atomistic/coarse-grained MD simulations in the near future. In all cases, trends of G' and G" showed the elastic solid-like behavior (G') of the samples to be predominant as compared to the viscous component (G") (Fig S1 a-b in the ESM). In subsequent frequency-sweep tests, G' profiles were almost unchanged along the tested frequency range (0.1-100 Hz) for both DCR-FAQ(LDLK)$_3$/gp (Fig. 2a$_I$) and ISCR-FAQ(LDLK)$_3$/gp (Fig. 2b$_I$) peptides, maintaining higher average G' values for FAQ(LDLK)$_3$/gp (170mM) as depicted in Fig. 2a$_{II}$-b$_{II}$ (p<0.05).

Failure strain and stress tests were also performed within the linear viscoelastic region to assess the hydrogels failure when subjected to a linear strain/stress progression. As expected, FAQ(LDLK)$_3$, yielding a soft hydrogel, showed a strain-to-failure of 8% (Fig. 2a$_{III}$). While the FAQ(LDLK)$_3$/gp peptides exhibited less deformation before failure than the soft self-assembled hydrogel, thus leading us to believe we had a more fragile "solid-like" structure. Indeed, the DCR-FAQ(LDLK)$_3$/gp exhibited a strain-to-failure of 2.9% and 3.5% respectively for 86mM and 170mM of genipin concentration (Fig. 2a$_{III}$); while the ISCR hydrogels with the 86mM and 170mM of genipin showed a strain failure of 2.7% and 3%, respectively (Fig. 2b$_{III}$). On the contrary the stiffening of the peptide chains, due to the cross-links, led to an increment of failure stress compared to the standard soft hydrogel. While failure occurred for a stress of 39 Pa for the FAQ(LDLK)$_3$, this was not the case for the DCR-FAQ(LDLK)$_3$/gp peptides, which failed at 1,738 Pa and 2,576 Pa respectively for 86mM and 170mM of genipin concentration (Fig. 2a$_{IV}$). An increase in failure stress was also observed in the ISCR-FAQ(LDLK)$_3$/gp, with failure occurring at stresses of 779 Pa (86mM) and 1,997 Pa (170mM) (Fig. 2b$_{IV}$). This manifold difference of stress failure (p<0.05), between cross-linked and un-cross-linked peptides (Fig. 2a$_V$-b$_V$) can be attributed to the efficient formation of covalent cross-links added to the standard weak intermolecular interactions already present in soft self-assembled hydrogels.

In the same way, we tested the possibility of lowering down the concentrations of genipin (ISPCR) to improve the biomechanics of FAQ(LDLK)$_3$ (1% w/v) partially (Fig. 3). For both ISPCR-FAQ(LDLK)$_3$ /gp peptides (14.6mM and 29.6mM) we found increments of G' values proportional to genipin concentrations (Fig. 3a) and always higher than G'' (Fig. S1c in the ESM), confirming a prevailing scaffold elastic component over the viscous one. The average G' values of ISPCR-FAQ(LDLK)$_3$/gp (14.6mM) and ISPCR-FAQ(LDLK)$_3$/gp (29.6mM) were 3.3 kPa and 4.8 kPa respectively (Fig. 3a$_I$). Both ISPCR-FAQ(LDLK)$_3$/gp exhibited a greater G' value (p<0.05) compared to FAQ(LDLK)$_3$ (Fig. 3a$_{II}$). In failure strain and stress tests both ISPCR-FAQ(LDLK)$_3$/gp exhibited a modest decrease of strain-to-failure (Fig. 3a$_{III}$) and an increment of their failure stresses (Fig. 3a$_{IV}$-a$_V$), likely due to the stiffening of cross-linked nanofibers.

Next, we looked at the stress-relaxation profile of the SAP-hydrogels. The rate of stress-relaxation under constant strain was quantified as the time for the initially measured stress to relax to half of its original value ($\tau_{½}$). We hypothesized that the stress-relaxation properties of the hydrogels could be modulated by using different cross-linker densities (170mM, 86mM and 14.6mM) on DCR and, as a consequence, different degrees of entanglement of the assembled peptides. Indeed, a low concentration of genipin gave a rate of stress-relaxation around 3.5s, whereas higher cross-linking density led to significantly longer timescale of $\tau_{½}$ ranging from 112 to 390 s (Fig. S2a in the ESM). Interestingly, the stress relaxation behavior of these materials closely fitted with a two-element Maxwell-Weichert linear viscoelastic model (Fig. S2a$_I$ in the ESM). Lastly, when temperature ramps were applied at physiological pH (Fig. S2b in the ESM), the solid-like DCR-FAQ(LDLK)$_3$/gp (170mM) gel did not turn into viscous-liquid state and G' remained constant, suggesting that the genipin-mediated cross-linking is not sensitive to temperature shifts within the tested temperature range.These results show that genipin could be a precious tool to modulate the mechanical properties of SAP-scaffolds, allowing to meet the needs of so far precluded different applications. Further, the tunability of their stress-relaxation profiles could be relevant for cell behavior studies since cells usually respond to oscillation forces in a few seconds, exert traction forces

on timescales of minutes, and undergo proliferation/spreading on minutes-to-hours timescales. [62]

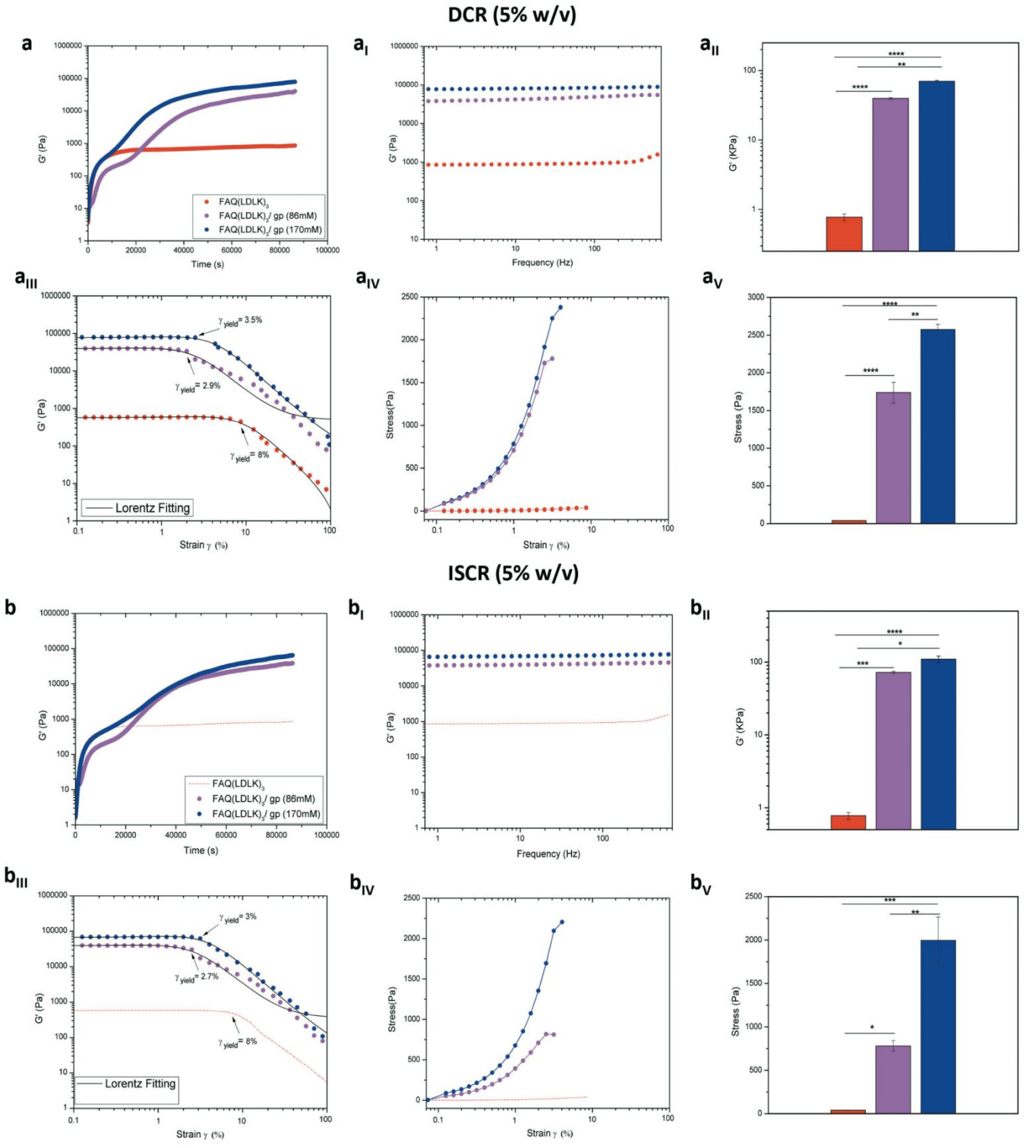

Figure 2. Rheological characterization of the DCR- and ISCR-FAQ(LDLK)$_3$/gp hydrogels. Peptide solutions were monitored via a 15 h time-sweep test (a-b) immediately after initiation of both self-assembly of FAQ(LDLK)$_3$ and cross-linking reaction (for DCR- and ISCR only), followed by a frequency sweep test (0.1-1,000 Hz). (a_I) Close to the equilibrium, FAQ(LDLK)$_3$ peptide had G' value of 0.7 kPa typical of soft SAP hydrogels, whereas the average G' values of DCR-FAQ(LDLK)$_3$/gp (86mM) and DCR-FAQ(LDLK)$_3$/gp (170mM) were 72 kPa and 110 kPa respectively. (b_I) For ISCR-FAQ(LDLK)$_3$/gp (86mM) and ISCR-FAQ(LDLK)$_3$/gp (170mM) the average G' values were respectively 39.5 kPa and 70 kPa. In both cases cross-linking led to a significant stiffness increase compared with the uncross-linked peptide (a_{II}-b_{II}) (n=3; p<0.05). In

strain-failure test (a_{III}-b_{III}), DCR- and ISCR-peptides were less prone to deformation than the soft self-assembled FAQ(LDLK)$_3$ hydrogel, due to their "solid-like" structure. In stress-failure tests (a_{IV}-b_{IV}), DCR- and ISCR-FAQ(LDLK)$_3$/gp showed a substantial failure stress increase compared with FAQ(LDLK)$_3$ (n=3) (a_V-b_V), likely thanks to the additional covalent interactions holding up the FAQ(LDLK)$_3$/gp self-assembled nanostructures.

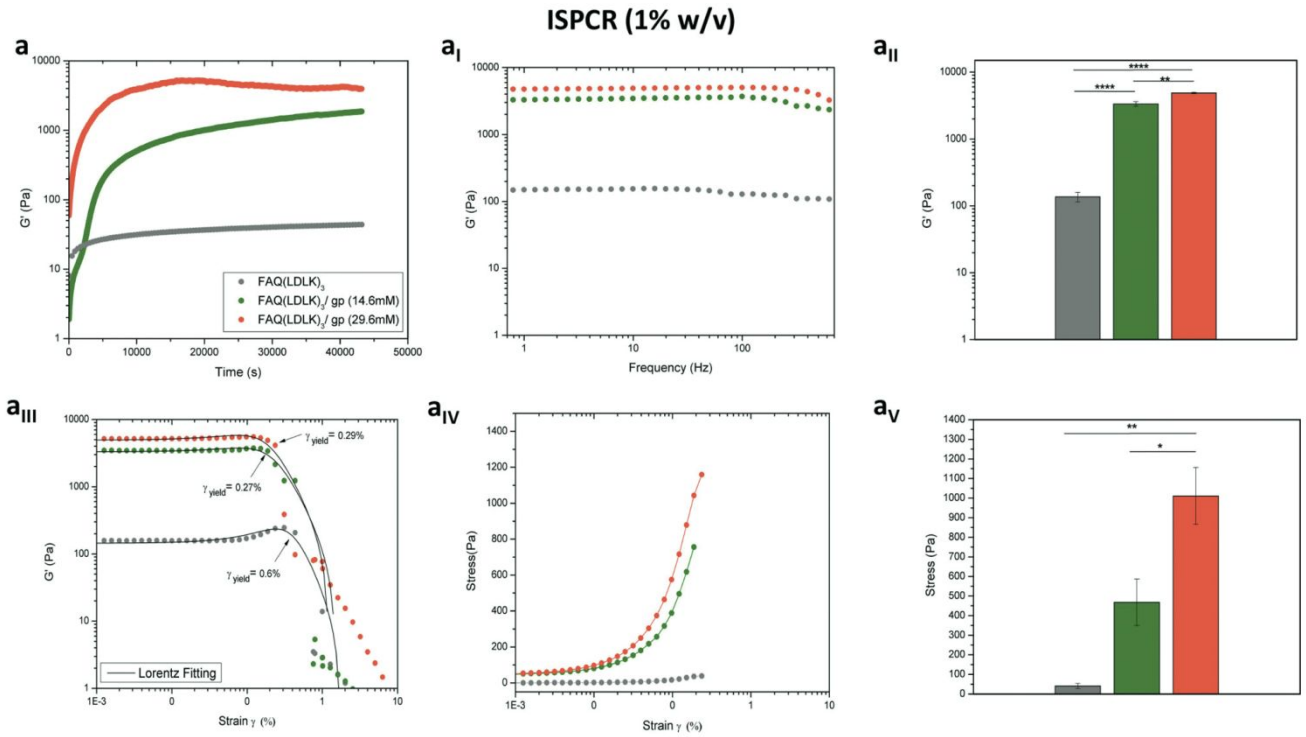

Figure 3. Rheological characterization of the ISPCR-FAQ(LDLK)$_3$/gp hydrogels. The improved biomechanics of ISPCR-FAQ(LDLK)$_3$ (1% w/v) at lower concentrations of genipin were monitored via time-sweep tests (a) followed by frequency sweep tests (0.1-1,000 Hz). The average G' of ISPCR-FAQ(LDLK)$_3$/gp (14.6mM) and ISPCR-FAQ(LDLK)$_3$/gp (29.6mM) were 3.3 kPa and 4.8 kPa respectively (a_I). Both ISPCR-FAQ(LDLK)$_3$/gp hydrogels exhibited greater G' values (n=3; $p<0.05$) compared to FAQ(LDLK)$_3$ (a_{II}). Failure strain and stress tests confirmed the previous findings at higher concentrations of genipin, i.e. both ISPCR-FAQ(LDLK)$_3$/gp exhibited decreased strain-to-failure (a_{III}) but increased failure stresses (a_{IV}-a_V) than soft FAQ(LDLK)$_3$ hydrogels (n=3; $p<0.05$) .

TNBSA assessment of cross-linking on SAP hydrogels

TNBSA was used to quantitatively measure the free primary amino groups during/after the cross-linking reaction to evaluate the reaction kinetics and the degree of cross-linking in genipin-treated SAP-hydrogels. TNBSA is a rapid and sensitive compound: it forms a highly chromogenic derivative, which can be measured at 335 nm. As expected, control FAQ(LDLK)$_3$ did not show changes over time, while both DCR- and ISCR-FAQ(LDLK)$_3$/gp displayed a decrease of free-amine groups during the cross-linking reaction (Fig 4). In DCR, free amine values of 43% and 28% were reached after 72h with 86mM and 170mM of genipin respectively (Fig. 4a). Instead, in ISCR, 51.7% and 35% free amine-groups weere detected after 72h, respectively for 86mM and 170mM (Fig. 4b). These different degrees of cross-linking corroborate the hypothesis that stiffness differences between the DCR- and ISCR-FAQ(LDLK)$_3$/gp can correlate to the different ways of interaction of genipin with respectively the already-assembled and the still-forming peptide nanostructures. At low concentrations of genipin, the reaction kinetic of ISPCR (Fig. 4c) was similar to those obtained with DCR and ISCR, with free amine values of 46.2% and 34.8% respectively for FAQ(LDLK)$_3$/gp (14.6mM) and FAQ(LDLK)$_3$/gp (29.6 mM).

The extent of the cross-linking reaction was also assessed via fluorescence measurements. In brief, the reaction of genipin compound with primary amines in peptides or proteins produces a blue pigmentation, [65] that qualitatively correlates with the degree of cross-linking and can be tracked analyzing its fluorescence (see fluorescence measurements section in Experiment for further details). When exposed to a clear solution of genipin, the initially translucent DCR (Fig. 4a_I) and ISCR (Fig. 4b_I) hydrogels gradually became light blue within a few hours, leading to a concomitant increase of fluorescence intensity. At 48h of cross-linking reaction fluorescence intensity got to the highest values and plateaued till after 72h. At this time-point a stable blue pigmentation was completely formed in all SAP-hydrogels, with the highest fluorescence values in samples with 170mM of genipin. A similar trend was observed in ISPCR as well (Fig. 4c_I). As expected, the fluorescence emission was not detected at 630 nm (λ_{ex}=590 nm) from the un-cross-linked FAQ(LDLK)$_3$ hydrogels. In addition, to assess whether the functional motif FAQRVPP could interact with genipin, thereby interfering with the cross-linking reaction, we monitored fluorescence intensity of the functional motif FAQRVPP in solutions of genipin. No fluorescence emission was observed during the time course of the reaction (data not shown), suggesting a poor, or even absent, interaction of genipin with the NH_2 group of

arginine (R) and/or the not-acetylated N-terminal of the chosen functional motif. Therefore we may assume a negligible interference of the cross-linking reaction with the biomimetic properties of original FAQ(LDLK)$_3$ peptide, already proved to be a promising candidate for the nervous tissue regeneration. [25] Nonetheless the effect of genipin cross-linking on functional motifs comprising lysine (K) should be carefully weighted as they indeed may take part to the cross-linking reaction.

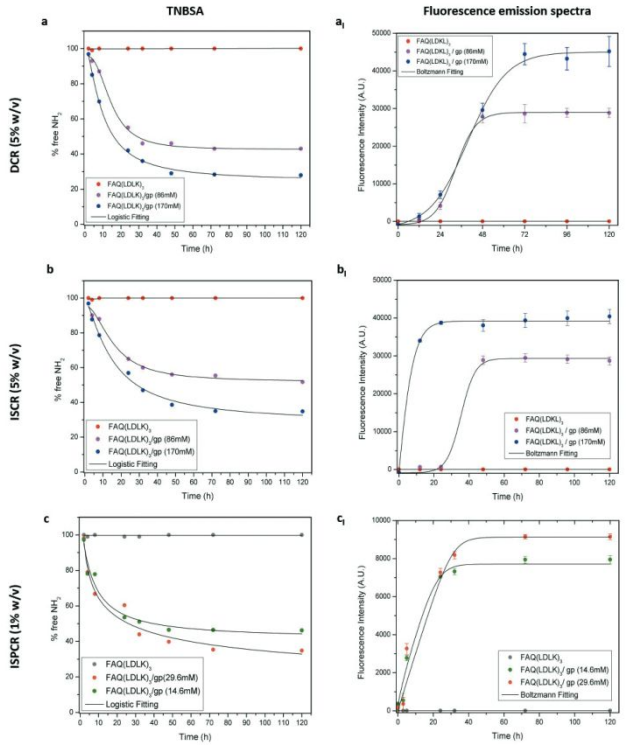

Figure 4. Cross-linking reaction kinetics: tracking the percentages of free primary amines of FAQ(LDLK)$_3$ and DCR-, ISCR- and ISPCR-FAQ(LDLK)$_3$/gp peptides over time. All peptide solutions were monitored by spectrophotometric TNBSA amines assay for 120 h. While control FAQ(LDLK)$_3$ (in red) did not display changes in free NH_2-groups over time, FAQ(LDLK)$_3$/gp peptides showed a decrease in free NH_2-groups during the time course of the reaction, related to genipin concentration and way of administration. (a) At 72 h DCR-FAQ(LDLK)$_3$/gp reached free amine values of 43% and 28% for 86mM and 170mM of genipin respectively. (b) Instead, in ISCR, 51.7% and 35% free amine-groups weere detected respectively for 86mM and 170mM. (c) By contrast, ISPCR-FAQ(LDLK)$_3$/gp at 14.6mM and 29.6 mM of genipin reached free-NH_2 values of 46.2% and 34.8%, respectively. The extent of the cross-linking reaction was also monitored via fluorescence measurements (a_l-b_l-c_l). The reaction of genipin compound with primary amines produces a blue pigmentation that correlates with the degree of cross-linking and can be tracked via fluorescence intensity measurements. Fluorescence intensity was recorded for FAQ(LDLK)$_3$, DCR-, ISCR- and ISPCR-FAQ(LDLK)$_3$/gp peptides from 0h to 120 h. No fluorescence emission was detected from the uncross-linked FAQ(LDLK)$_3$ hydrogels (in red). On the contrary, DCR-, ISCR- and ISPCR-FAQ(LDLK)$_3$/gp peptides led to an increase of fluorescence intensity during the time course of the reaction. At 72h a stable blue pigmentation was completely formed in all cross-linked SAP-hydrogels.

Influence of cross-linking on assembled secondary structures

Structural characterization of assembled SAPs was pursued by ATR-FTIR. β-sheet structures can be tracked by analyzing the Amide I region (1,600-1,700 cm^{-1}), which is mainly associated with C=O stretching vibration and related to the SAP-backbone conformation. Conventionally, in parallel β-sheet structures, the Amide I region exhibits a peak around 1,630 cm^{-1}, while in anti-parallel β-sheet structures the Amide I region displays both a major component at 1,630 cm^{-1} and a minor component at 1,695 cm^{-1}. The ratio of peak intensities at 1,695 cm^{-1} and 1,630 cm^{-1}, named β-sheet organizational index, is proportional to the ratio of antiparallel/parallel β-sheet structures. [86] FTIR spectra of FAQ(LDLK)$_3$, showed anti-parallel β-sheet features (β-sheet organizational index= 21.6%). A predominantly anti-parallel β-sheet structure was seen also in the DCR-FAQ(LDLK)$_3$/gp, with a slight variation of the β-sheet organizational index in FAQ(LDLK)$_3$/gp (86mM) and (170mM), i.e. 16.32% and 19.65% respectively (Fig. 5a). In contrast, β-sheet bands in ISCR-FAQ(LDLK)$_3$/gp were still present but the Amide I peak decreased and broadened, likely due to NH_2-group deformation (Fig. 5b). In both ISCR-FAQ(LDLK)$_3$/gp peptides, the β-sheet organizational index significantly decreased compared to FAQ(LDLK)$_3$, showing values of 13.68% and 15.63% respectively for 86mM and 170mM of genipin. This decrease in β-structuring, highlights that in ISCR, since the cross-linking reaction is concomitant with the self-assembly phenomenon, the genipin could affect the stabilizations of the forming β-sheet domains, thus influencing not only the mechanical strength of the resulting SAP-hydrogels, as previously observed in biomechanical characterization, but also their macromolecular organization. In the Amide II region (1,480-1,575 cm^{-1}), β-sheet aggregation for all tested SAPs was confirmed by the presence of a peak at ≈1,543 cm^{-1} directly related to CN stretching and NH bending.

In addition, we assessed NH stretching in the 3,100-3,300 cm^{-1} region, where primary amines (R-NH_2) features two bands, due to the asymmetrical and symmetrical NH stretch respectively. Instead, secondary amines (R_2-NH) show only a single weak and broad band given by their single NH bond. FAQ(LDLK)$_3$ peptide displayed two peaks ascribable to primary amines stretching, while DCR- and ISCR-FAQ(LDLK)$_3$/gp showed only one NH-stretch (Fig 5a_l-b_l). Hence, these features suggest that the carboxymethyl groups of genipin reacted with the primary amino-groups of SAPs yielding to secondary amines.

FTIR spectra of ISPCR-FAQ(LDLK)$_3$/gp showed β-sheet features in Amide I and II regions, characterized by the presence of peaks at 1,620, 1,695 and 1,543 cm^{-1} (Fig. 5c). However, it has to be noted that β-sheet signature appeared more evident and similar to those of FAQ(LDLK)$_3$, suggesting that low concentrations of genipin and a shorter reaction time moderately influence the β-sheet formation propensity of the tested SAP. Lastly, primary amine peaks are still present in the 3,100-3,300 cm^{-1} band (Fig. 5c_l), likely because of a partial linking of the free amine groups in a cross-linking reaction of just 24 hours.

X-ray diffraction characterization

In X-ray diffraction analyses (see Experiment for details) the first low Q peaks (d= 3.9 nm in Fig. 5d-d_I) matched the SAP fibers heights obtained with AFM tests (see next paragraph and Fig. S3a in the ESM). Peaks at 2.4 nm and at 1.2 nm likely pointed at respectively the total thickness and at the intra-layers distance of typical bilayered β-sheet structures found in similar SAPs. [87] The peak at 0.6 nm could be assigned to the length of the lysine side-chain, while the strong peak at 0.45 nm was ascribable to the peptide backbone distance in β-sheets.[88] $FAQ(LDLK)_3$/gp peptides displayed a significant increment of the latter peak, correlated to the concentration of genipin: this was probably due to stronger backbone packing after cross-linking. Lastly, the 0.327 nm spacing could be ascribed to the distance among residues along peptide chains. Based on these results we hypothesize that cross-linking presumably strengthened up peptide backbone packing, and significantly contributed to the stabilization of assembled structures without affecting the standard SAP assembling into cross-β structures. [35]

Morphological characterization

Atomic force microscope (AFM) morphological analysis was carried out to monitor the effects of cross-linking on the self-aggregated nanostructures of $FAQ(LDLK)_3$ peptides. All tested peptides self-assembled into nanofibers but with slightly different morphologies. $FAQ(LDLK)_3$ yielded short and single fibers with ≈13 nm in width, consistent with those previously obtained (Fig 6a).[26] $FAQ(LDLK)_3$ height ranged from 2.4 to 3.9 nm (Fig. S3a in the ESM), in agreement with data obtained from XRD analysis. By contrast, nanofibers morphology of DCR-$FAQ(LDLK)_3$/gp featured a tight and clustered bundles network of presumably cross-linked nanofibers: average values of 14.63 nm and 3.16 nm in width and height respectively. Instead, ISCR-$FAQ(LDLK)_3$/gp (Fig 6b) showed fibers less tangled and more similar to those of $FAQ(LDLK)_3$ (Fig. 6c).
AFM results confirmed the assembly propensity of all peptides into nanofibers and suggested that genipin cross-linking have fostered the formation of clusters of nanofibers.

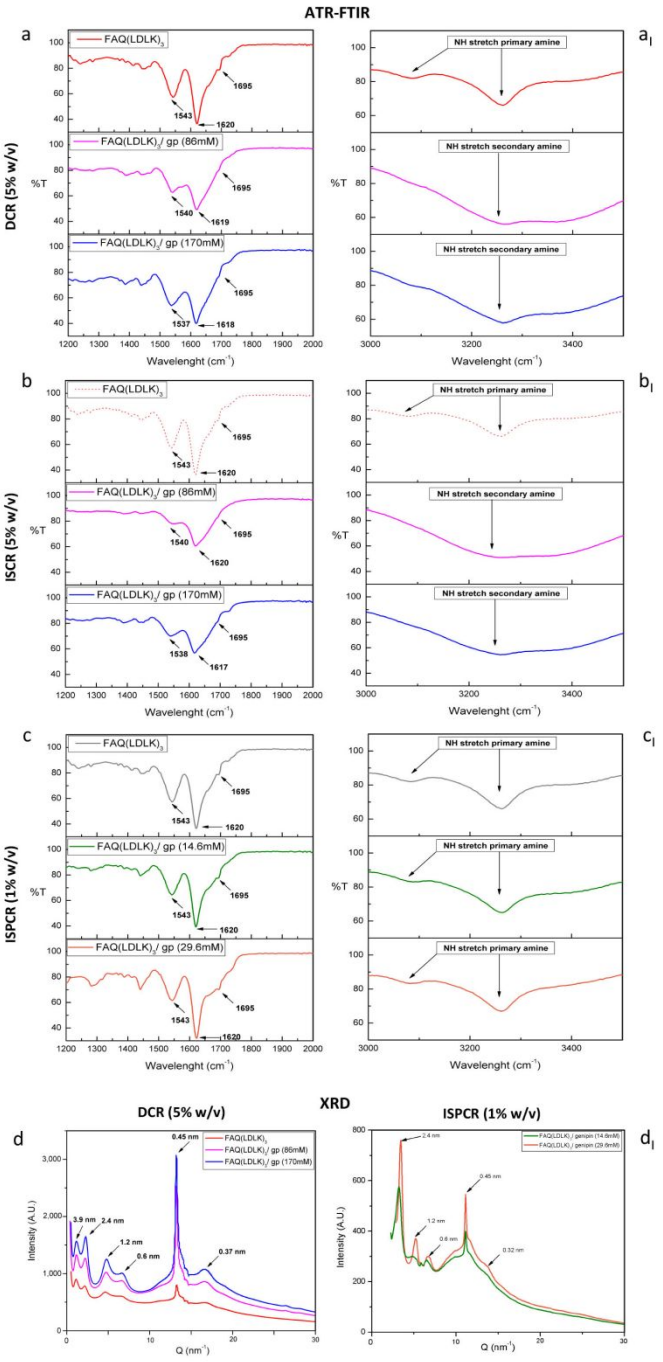

Figure 5. Structural characterization of assembled scaffolds. ATR-FTIR spectra in the Amide I and Amide II absorption regions of DCR-$FAQ(LDLK)_3$/gp (a), ISCR-$FAQ(LDLK)_3$/gp (b) and ISPCR-$FAQ(LDLK)_3$/gp (c). All peptides spectra displayed a broad band near 1,540 cm^{-1} (Amide II region,β-sheet aggregation) and peaks at 1,620 and 1,695 cm^{-1} (Amide I region, antiparallel β-sheet structures). In addition, NH stretching in the 3,100-3,300 cm^{-1} band has been assessed. $FAQ(LDLK)_3$ peptide displayed two peaks ascribable to primary amines stretching, while DCR- and ISCR-$FAQ(LDLK)_3$/gp showed only one peak (a_I-b_I), suggesting that the carboxymethyl group of genipin reacted with the majority of the primary amino-groups of SAPs, yielding to secondary amines. In ISPCR-

FAQ(LDLK)$_3$/gp (c_l) peaks assigned to primary amines are still detectable, likely due to the partial linking of the free amine groups after a crosslinking reaction run for just 24 hours. (d-d_l) X-ray diffraction (XRD) data of FAQ(LDLK)$_3$ (red), DCR-FAQ(LDLK)$_3$/gp 86mM (magenta), DCR-FAQ(LDLK)$_3$/gp 170mM (blue), ISPCR-FAQ(LDLK)$_3$/gp 14.6mM (green), and ISPCR-FAQ(LDLK)$_3$/gp 29.6mM (orange); all of these SAPs show similar XRD peaks, suggesting the presence of similar structures.

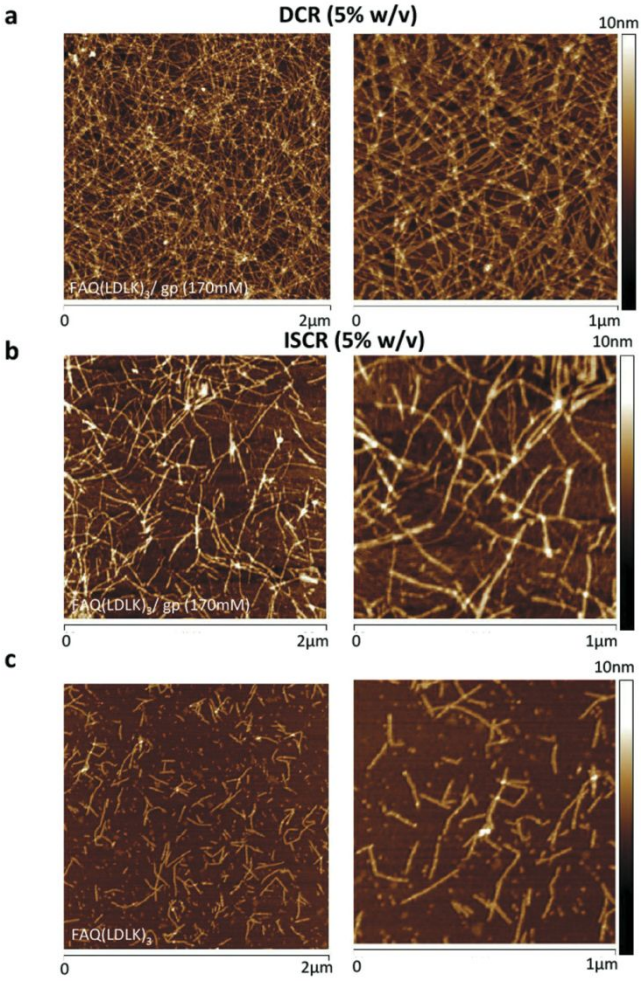

Figure 6. Atomic force microscope (AFM) morphological analysis. (a) DCR-FAQ(LDLK)$_3$/gp self-organized into a tight and clustered network of 14.63 nm-wide and 3.16 nm-long nanofibers. Instead, ISCR-FAQ(LDLK)3/gp (b) showed a fiber morphology less tangled. (c) FAQ(LDLK)$_3$ self-assembled into single short nanofibers.

***In vitro* degradation of cross-linked hydrogels**

Weight loss of hydrogels upon exposure to trypsin digestion (at 37°C) was used to test the degradation of assembled SAPs. All samples showed significant weight loss over time (Fig. S4a in the ESM). The weight of FAQ(LDLK)$_3$ peptide decreased faster than those of cross-linked samples, showing 86% of degradation after 4 weeks. Both FAQ(LDLK)$_3$/gp at 14.6mM and 170mM of genipin, needed 8-10 weeks respectively to be degraded to that value. Indeed, the weight loss rate of these samples was relatively constant throughout the degradation test; however, a total degradation was not observed in either cross-linked samples. It is interesting to report the morphological differences arose during degradation tests: in FAQ(LDLK)$_3$/gp (170mM), trypsin-mediated degradation was evenly distributed on the sample surface, leading to an increase in surface roughness and a significant decrease in the hydrogel thickness from 2 mm to 0.5 mm after 6 weeks. On the contrary, the digestion of the FAQ(LDLK)$_3$/gp (14.6mM) was more localized in the central part of the hydrogel.

Since particulate debris was present in the supernatant, this was analyzed to evaluate the presence of both degraded peptides and genipin released during degradation. In absorbance measurements, all tested SAPs exhibited the typical 230 nm and 270 nm peaks of peptide bond and aromatic amino acids respectively. Instead, in fluorescence measurements (see Experiment for details) we detected the presence of genipin released during the trypsin degradation experiment (data not shown).

We also evaluated the behavior of the genipin cross-linked SAPs in the presence of organic solvents (such as dichloromethane, dimethylformamide, chloroform, methanol), that usually lead to dissolution of PCL, PLGA and PLA polymers. When genipin cross-linked SAPs were dipped in these solutions for 48 h, they did not show changes in terms of degradation, dissolution or shrinkage: an interesting quality of cross-linked SAPs (not present in standard soft SAPs) which can be taken into account to design composite materials made of polymers/functionalized peptides or to develop novel SAP casting protocols.

Fabrication and characterization of electrospun cross-linked nanofibrous scaffolds

In the last two decades, electrospinning technique has emerged as a promising approach for large-scale production of nanofibers. Among other qualities, electrospinning allows for the fabrication of well-defined 3D porous nano- and micro-fibrous scaffolds, an asset useful for many TE applications, [33, 89-93] but currently missing in all SAP-made scaffolds. So far electrospinning has been mainly used for natural and synthetic polymers but, as such, electrospun fibrous scaffolds do not feature an easiness of functionalization with bioactive peptides comparable to SAPs. Indeed, biomimetic scaffolds coaxing specific cell behaviors like, for example, migration, differentiation and proliferation have become a hot topic in TE. [94]

In order to overcome this issue, modification of electrospun fibrous scaffolds with the incorporation of bioactive molecules (i.e. RGD, YIGSR, IKVAV or FAQRVPP) using covalent binding,[95-97] noncovalent host–guest interactions,[98] physical adsorption (plasma-treatment)[99] or blended electrospinning procedures,[33] became interesting strategies to mimic the biochemical properties of the ECM, thus creating biomimetic scaffolds fostering tissue regeneration at the site of implant. However, to take full advantage of the several benefits coming from SAP-technology (e.g. multi-functionalization, high biocompatibility, pathogen-free, easiness of production and tailoring, etc.) researchers moved their efforts toward the ES of pure SAPs, [34, 100] unfortunately obtaining just soft fibrous-based SAP coatings because of the poor mechanical properties of peptides. Driven by the idea that scaffolds should be designed both at the biochemical and biomechanical levels we successfully applied the cross-linking technique to nanofibrous electrospun scaffolds to obtain, for the first time, flexible self-standing 3D scaffolds made of pure SAPs (Fig. 7a)

Our ES studies suggested that DCR was not feasible with electrospinning of FAQ(LDLK)$_3$ as electrospun nanofibers dissolved in aqueous post-treatment solutions before cross-linking was

consolidated (data not shown). On the other hand, only low concentration of genipin could be added to the starting ES solution in order to prevent gelling and clogging of ES setup. The best method developed for FAQ(LDLK)$_3$/gp fibers fabrication was based on ISPCR-FAQ(LDLK)$_3$ with 14.6mM of genipin.

We focused our efforts on the fabrication of fibrous mats and micro-channels as described in the Experiment section. After electrospinning, ISPCR-FAQ(LDLK)$_3$/gp fibers were white in color with both round and flat shapes (Fig 7a$_{I}$). As previously described, ISPCR kinetics told us some genipin inside the fibers could be still activated in subsequent post-treatment (PT) steps. Firstly, the white electrospun fibers were exposed to the vapor phase of 2.5mM of NaOH in PBS (PT-I) at 37°C for 3 days in order to slightly activate the cross-linking reaction and stabilize the fibers morphology. As this step was not enough to provide stable scaffolds a post-treatment through immersion in high-concentrated genipin solution was added to achieve a higher degree of cross-linking. Hence, the partially cross-linked fibers were immersed in 170mM of genipin in H_2O:EtOH (90:10 v/v) for 1 day at 37°C (PT-II), and finally soaked in PBS for 1 day (PT-III) to remove any remnants of ethanol. After each PT-step, the increase of cross-linking degree was testified by the appearance and increase of a darker blue color throughout the procedures (Fig. 7a$_{II}$). Overall, PT-steps lead to a latitude shrinkage of the FAQ(LDLK)$_3$/gp scaffolds, but they preserved its interconnected-porous 3D fibrous network (Fig. S5 in the ESM). As shown in SEM images of ISPCR-FAQ(LDLK)$_3$/gp of PT (Fig. 7b), fibers were randomly oriented giving a very porous construct with average fiber diameters of 294 nm. Interestingly, a significant number of linked fibers in the fiber-to-fiber interconnections was observed in the junctions of adjacent fibers for electrospun FAQ(LDLK)$_3$/gp after PT. This feature made a stable 3D-interconnected network structure with preserved fibrous morphology. Notably, the fibers were not merged before PT (Fig. S6 in the ESM).

The obtained fibrous scaffolds were characterized through ATR-FTIR tests. Before PT electrospun FAQ(LDLK)$_3$/gp showed a 1,654 cm^{-1} peak in the Amide I region (1,600-1,700 cm^{-1}) mainly related to random coil conformations; whereas in the Amide II region (1,480-1,575 cm^{-1}) it exhibited a broad peak at 1,540 cm^{-1} ascribable to β-sheets aggregation (Fig. 7c). In contrast, narrow characteristic peaks at 1,627 cm^{-1} (Amide I) and 1,530 cm^{-1} (Amide II) showed stronger β-sheet formation of FAQ(LDLK)$_3$/gp after PT (Fig. 7c$_{I}$), highlighting that the PT-steps influence not only the cross-linking reaction but also the macromolecular organization of the resulting electrospun SAP-fibers. Uncross-linked electrospun FAQ(LDLK)$_3$ revealed broader bands (with relatively less intensity) centered near 1,654 cm^{-1} and 1,540 cm^{-1} which were characteristic of mainly random coil and β-sheet conformations, respectively (data not shown). Further, mechanical characterization was performed on cross-linked electrospun FAQ(LDLK)$_3$/gp nanofibrous mats having two different thickness, after the PT-steps. Electrospun mats were cut into a rectangular shape (50 mm × 30 mm; thickness = 0.185 mm or 0.36 mm) and placed on the rheometer plate. Storage (G') and loss modulus (G") were measured by varying frequencies of applied oscillatory stress. The average G' and G" values were respectively of 2.095 kPa and 50 Pa for the electrospun mats with 0.185 mm of thickness, whereas of 7.365 kPa and 394.7 Pa for the electrospun mats with 0.36 mm of thickness (Fig. S7a in the ESM). As expected, mechanical properties well-correlate with the overall scaffold thickness due to the increased concentration of entangled nanofibers and covalent binding. For both the FAQ(LDLK)$_3$/gp nanofibrous mats, G'/G" remained relatively constant along the tested frequency range (0.1-1,000 Hz) suggesting that the electrospun scaffolds are resistant to deformations applied at different oscillatory frequencies. Stress/strain failure was also performed (0.1%-1,000% strain) to identify the maximum strain/stress to which the sample can be subjected. The electrospun FAQ(LDLK)$_3$/gp nanofibrous mats (thickness = 0.185 mm) showed a strain-to-failure of 57.82% with a failure stress occurred at 509 Pa; instead the electrospun FAQ(LDLK)$_3$/gp nanofibrous mats (thickness = 0.36 mm) exhibited a strain-to-failure of 108.2% with a failure stress at 1130 Pa (Figure S7b in the ESM). These values of strain-to-failure are particularly interesting as, to the best of our knowledge, they have never been reached with SAP-based scaffolds so far and are desirable features for deformable biomaterials to be used in tissue engineering. Nonetheless, this mechanical behavior of electrospun cross-linked constructs is comparable with previous reports of polymeric electrospun nanofibrous mats.[33, 101] Lastly, temperature ramps were recorded as a function of G' (see Experiment for further details). When temperature ramps were applied to the electrospun FAQ(LDLK)$_3$/gp nanofibrous mats, a phase transition was not observed and the G' remained constant through the tested temperature range (Figure S7c in the ESM) similarly to the DCR-FAQ(LDLK)3/gp membrane, highlighting their stability when subjected to temperature increments.

Moreover, as ES solution came from ISPCR-SAPs, the cross-linker was likely well-distributed within the electrospun FAQ(LDLK)$_3$/gp fibers: this led to the manufacture of a single unified, self-standing tubular channel with spring-like properties (e.g. recoverable deformation under load) (Video S2 in the ESM). Furthermore, contrarily to uncross-linked FAQ(LDLK)$_3$, electrospun fibers of FAQ(LDLK)$_3$/gp were stable in wet state (upon exposure to PBS at 37°C) over time (Fig. S8 in the ESM), allowing for their long-term use. Also, after cross-linking, electrospun SAP scaffolds showed an interesting stability (data not shown) in different organic solvents, unusual of standard electrospun SAPs.

Taken together, these results make electrospun scaffolds from FAQ(LDLK)$_3$/gp particularly promising candidates for tissue engineering applications thanks to their stable 3D fibrous-based structure capable of retaining fiber morphology when immersed in aqueous solutions and/or when subjected to external deformations.

Cell Morphology and Viability Assays

Since the system investigated here has structural features that are biomimetic of ECMs, and can also providing functionalized microenvironment with specific biological cues capable of stimulating adult neural stem cell adhesion and differentiation,[26] we chose to investigate if genipin can have cytotoxic effects on hNSCs and how organization of the cross-linked electrospun fibers affects cells in culture. We selected GMP-grade hNSCs for these experiments, since they are well-know and characterized on SAP scaffolds,[25, 35, 68, 71, 102, 103] but also because it is documented their therapeutic efficacy as safe cell therapy approach for a phase I clinical trial of Amyotrophic Lateral Sclerosis (ALS).[70]

To evaluate whether genipin can affect the hNSCs viability, different genipin concentrations (21mM, 42mM and 64mM) were added to the cell culture medium and incubated for one day at 37°C (see Experiment for further details). Cell viability was found to be high in each of tested conditions (Figure S9a in the ESM), suggesting a negligible cytotoxicity ascribable to genipin. We next investigated whether cross-linked electrospun scaffolds made of functionalized FAQ(LDLK)$_3$/gp could be still considered biomimetic scaffolds for their future use in neural tissue engineering applications. After

7DIV, we assessed the phenotype of differentiated hNSC progenies cultured on the top surface of es-FAQ(LDLK)$_3$/gp scaffolds (Figure S9b in the ESM). hNSC differentiated progeny was immunostained with markers for astrocytes (GFAP), post-mitotic neurons (βIII-Tubulin) and oligodendrocytes (GalC and O4). hNSCs cultured on cross-linked electrospun scaffolds exhibited a spread and branching neural morphology similar to that one found on previously reported FAQ(LDLK)$_3$ hydrogel.[26]

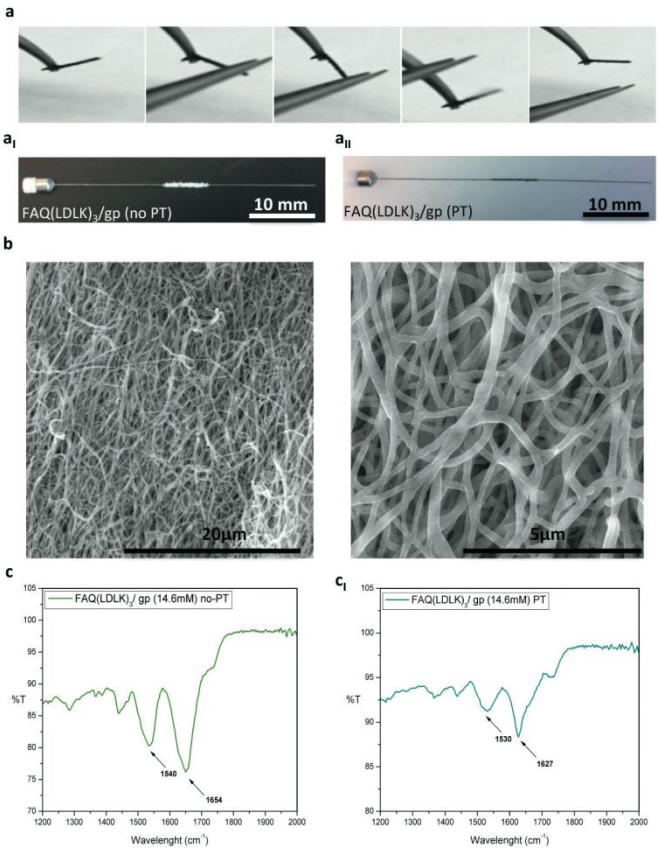

Figure 7. (a) Self-standing electrospun microchannels made of the ISPCR-FAQ(LDLK)$_3$/gp (14.6 mM, 72h) peptide. (a$_I$) After electrospinning, ISPCR-FAQ(LDLK)$_3$/gp fibers were white in color (no-PT), whereas after PT ISPCR-FAQ(LDLK)$_3$/gp fibers appeared dark-blue due to the increase of the cross-linking degree (a$_{II}$). Even if PT-steps led to a latitude shrinkage of the ISPCR-FAQ(LDLK)$_3$/gp microchannel, they preserved its interconnected-porous 3D fibrous network. (b) SEM images of ISPCR-FAQ(LDLK)$_3$/gp fibers after PT at low and high magnifications. ISPCR-FAQ(LDLK)$_3$/gp fibers were randomly oriented, giving a very porous construct with average fiber diameters of 294 nm. ATR-FTIR spectra in the Amide I and Amide II absorption regions of electrospun ISPCR-FAQ(LDLK)$_3$/gp before and after PT. (c) electrospun ISPCR-FAQ(LDLK)$_3$/gp before PT showed a peak at 1,654 cm^{-1} related to random coil conformations; whereas in the Amide II region it exhibited a broad peak at 1,540 cm^{-1} ascribable to β-sheets aggregation. (c$_I$) Electrospun ISPCR-FAQ(LDLK)$_3$/gp after PT showed peaks at 1,627 cm^{-1} (Amide I) and at 1,530 cm^{-1} (Amide II) indicative of a stronger β-sheet formation, highlighting that PT-steps influenced the cross-linking reaction and also the macromolecular organization of the resulting electrospun SAP-fibers.

Conclusions

Over the last two decades self-assembling peptides came under the spotlight because of their ease of design, functionalization and synthesis. They showed promising potential in regenerative therapies as soft hydrogels, but so far lacked biomechanical properties required for their engraftment into medium-hard tissues and for the production of complex 3D scaffolds typical of polymers and natural cross-linked proteins.

In this work we developed a feasible cross-linking strategy to modulate the mechanical properties of biomimetic SAPs and we introduced different genipin cross-linking protocols with profound effect on stiffness, bioabsorption time and molecular arrangements of scaffolds. Biomechanical enhancements were dependent on dose and time of exposure to genipin, thus allowing their tuning to suit the specific needs of different applications. We showed the cross-linking reaction did not involve the residues of the chosen functional motifs, thus leaving the door open to crosslinking of multi-functionalized SAPs. In addition, thanks to the improved SAP chain length and biomechanics, we managed, for the first time, to electrospin the cross-linked SAPs into single unified and self-standing mats and microchannels having interconnected fibers. Indeed, our electrospun highly cross-linked SAP constructs retained their fibrous morphology when immersed in aqueous solution, showing flexibility, spring-like behaviour and better stability to degradation. Lastly, evidence of preserved functional motif bioactivity was established by detecting the three main phenotypes and respective morphologies of differentiated hNSC progenies on the surface of electrospun cross-linked nanofibrous scaffolds (Fig.S9).

This work may open the door to the development and tailoring of functionalized synthetic bioprostheses entirely made of SAPs with tunable resilience, bioabsorption times and/or bioactivities for different tissue engineering applications and beyond.

Conflicts of interest

There are no conflicts to declare.

Author contributions

R.P. and F.G. conceived the project. R.P. synthesized the peptides and carried out the hydrogel cross-linking experiments while M.M. took care of the electrospinning ones. F.G. supervised the project. R.Z. co-supervised XRD experiments. R.P. and F.G. wrote the manuscript. All authors have approved the final article.

Orcid

R.Pugliese https://orcid.org/0000-0001-7669-4457 ;

M. Maleki https://orcid.org/0000-0001-5746-4736 ;

R.N. Zuckermann https://orcid.org/0000-0002-3055-8860 ;

F. Gelain https://orcid.org/0000-0002-2624-5853 ;

Acknowledgements

Work described and performed by R.P., M.M. and F.G. was funded by the ''Ricerca Corrente" funding granted by the Italian Ministry of Health and by the ''5x1000" voluntary contributions. Financial support also came from Revert and Vertical Onlus donations. XRD experiments were conducted at the Advanced Light Source and at the Molecular Foundry (The Lawrence Berkeley National Laboratory) both of which are supported by the Office of Science, under Contract No. DE-AC02-05CH11231. We thank Amanda Marchini for running all the in vitro experiments assessing cytotoxicity and differentiation of hNSC on cross-linked substrates. We thank Prof. Luca Beverina for allowing our FTIR experiments to be performed at his facility at the Material Science Dept. of the University of Milan-Bicocca.

References

1. S. Zhang, *Interface focus*, 2017, **7**, 20170028.
2. B. B. Hsu, W. Conway, C. M. Tschabrunn, M. Mehta, M. B. Perez-Cuevas, S. Zhang and P. T. Hammond, *ACS nano*, 2015, **9**, 9394-9406.
3. S. Yang, S. Wei, Y. Mao, H. Zheng, J. Feng, J. Cui, X. Xie, F. Chen and H. Li, *BMC biotechnology*, 2018, **18**, 12.
4. C. E. Morgan, A. W. Dombrowski, C. M. Rubert Perez, E. S. Bahnson, N. D. Tsihlis, W. Jiang, Q. Jiang, J. M. Vercammen, V. S. Prakash, T. A. Pritts, S. I. Stupp and M. R. Kibbe, *ACS nano*, 2016, **10**, 899-909.
5. M. Zhao, Y. Zhou, S. Liu, L. Li, Y. Chen, J. Cheng, Y. Lu and J. Liu, *Drug delivery*, 2018, **25**, 546-554.
6. Z. Song, X. Chen, X. You, K. Huang, A. Dhinakar, Z. Gu and J. Wu, *Biomaterials science*, 2017, **5**, 2369-2380.
7. A. Zhou, S. Chen, B. He, W. Zhao, X. Chen and D. Jiang, *Drug design, development and therapy*, 2016, **10**, 3043-3051.
8. C. Karavasili, M. Spanakis, D. Papagiannopoulou, I. S. Vizirianakis, D. G. Fatouros and S. Koutsopoulos, *Journal of pharmaceutical sciences*, 2015, **104**, 2304-2311.
9. M. Ozeki, S. Kuroda, K. Kon and S. Kasugai, *J Biomater Appl*, 2011, **25**, 663-684.
10. H. Nakahara, H. Misawa, A. Yoshida, T. Hayashi, M. Tanaka, T. Furumatsu, N. Tanaka, N. Kobayashi and T. Ozaki, *Cell transplantation*, 2010, **19**, 791-797.
11. B. He, Y. Ou, S. Chen, W. Zhao, A. Zhou, J. Zhao, H. Li, D. Jiang and Y. Zhu, *Materials science & engineering. C, Materials for biological applications*, 2017, **74**, 451-458.
12. A. Schneider, J. A. Garlick and C. Egles, *PloS one*, 2008, **3**, e1410.
13. F. Paladini, S. T. Meikle, I. R. Cooper, J. Lacey, V. Perugini and M. Santin, *Journal of materials science. Materials in medicine*, 2013, **24**, 2461-2472.
14. Y. Loo, Y. C. Wong, E. Z. Cai, C. H. Ang, A. Raju, A. Lakshmanan, A. G. Koh, H. J. Zhou, T. C. Lim, S. M. Moochhala and C. A. Hauser, *Biomaterials*, 2014, **35**, 4805-4814.
15. Y. Ichihara, M. Kaneko, K. Yamahara, M. Koulouroudias, N. Sato, R. Uppal, K. Yamazaki, S. Saito and K. Suzuki, *Biomaterials*, 2018, **154**, 12-23.
16. M. Zhang, W. W. Ai, Z. L. Mei, Y. H. Hu and Z. L. Zhang, *Experimental and therapeutic medicine*, 2017, **14**, 3441-3446.
17. M. E. Davis, J. P. Motion, D. A. Narmoneva, T. Takahashi, D. Hakuno, R. D. Kamm, S. Zhang and R. T. Lee, *Circulation*, 2005, **111**, 442-450.
18. B. He, X. Yuan, A. Zhou, H. Zhang and D. Jiang, *Expert reviews in molecular medicine*, 2014, **16**, e12.
19. J. Kisiday, M. Jin, B. Kurz, H. Hung, C. Semino, S. Zhang and A. J. Grodzinsky, *Proceedings of the National Academy of Sciences of the United States of America*, 2002, **99**, 9996-10001.
20. X. C. Li, Y. H. Wu, X. D. Bai, W. Ji, Z. M. Guo, C. F. Wang, Q. He and D. K. Ruan, *Tissue engineering. Part A*, 2016, **22**, 1218-1228.
21. Y. Wu, Z. Jia, L. Liu, Y. Zhao, H. Li, C. Wang, H. Tao, Y. Tang, Q. He and D. Ruan, *Artificial organs*, 2016, **40**, E112-119.
22. P. A. Brunton, R. P. Davies, J. L. Burke, A. Smith, A. Aggeli, S. J. Brookes and J. Kirkham, *Br Dent J*, 2013, **215**, E6.
23. M. Schlee, F. Rathe, C. Bommer, F. Broseler and L. Kind, *Journal of periodontology*, 2018, DOI: 10.1002/JPER.17-0429.
24. Y. Kondo, T. Nagasaka, S. Kobayashi, N. Kobayashi and T. Fujiwara, *Hepato-gastroenterology*, 2014, **61**, 349-353.
25. A. Caprini, D. Silva, I. Zanoni, C. Cunha, C. Volonte, A. Vescovi and F. Gelain, *New biotechnology*, 2013, **30**, 552-562.
26. F. Gelain, D. Cigognini, A. Caprini, D. Silva, B. Colleoni, M. Donega, S. Antonini, B. E. Cohen and A. Vescovi, *Nanoscale*, 2012, **4**, 2946-2957.
27. S. Koutsopoulos, L. D. Unsworth, Y. Nagai and S. Zhang, *Proceedings of the National Academy of Sciences of the United States of America*, 2009, **106**, 4623-4628.

28. F. Gelain, L. D. Unsworth and S. Zhang, *J Control Release*, 2010, **145**, 231-239.
29. R. Pugliese and F. Gelain, *Trends in biotechnology*, 2017, **35**, 145-158.
30. S. Panseri, C. Cunha, J. Lowery, U. Del Carro, F. Taraballi, S. Amadio, A. Vescovi and F. Gelain, *BMC biotechnology*, 2008, **8**, 39.
31. T. T. Yuan, A. M. DiGeorge Foushee, M. C. Johnson, A. R. Jockheck-Clark and J. M. Stahl, *Nanoscale research letters*, 2018, **13**, 88.
32. S. Hong and G. Kim, *Journal of biomedical materials research. Part B, Applied biomaterials*, 2010, **94**, 421-428.
33. A. Raspa, A. Marchini, R. Pugliese, M. Mauri, M. Maleki, R. Vasita and F. Gelain, *Nanoscale*, 2016, **8**, 253-265.
34. M. Maleki, A. Natalello, R. Pugliese and F. Gelain, *Acta biomaterialia*, 2017, **51**, 268-278.
35. R. Pugliese, A. Marchini, G. A. A. Saracino, R. N. Zuckermann and F. Gelain, *Nano Research*, 2018, **11**, 586–602.
36. S. Habtemariam and G. Lentini, *Biomedicines*, 2018, **6**.
37. G. Chen and X. Guo, *International review of neurobiology*, 2017, **135**, 77-95.
38. A. Bigi, G. Cojazzi, S. Panzavolta, N. Roveri and K. Rubini, *Biomaterials*, 2002, **23**, 4827-4832.
39. G. Yang, Z. Xiao, H. Long, K. Ma, J. Zhang, X. Ren and J. Zhang, *Scientific reports*, 2018, **8**, 1616.
40. P. Sanchez, J. L. Pedraz and G. Orive, *International journal of biological macromolecules*, 2017, **98**, 486-494.
41. J. Berger, M. Reist, J. M. Mayer, O. Felt, N. A. Peppas and R. Gurny, *European journal of pharmaceutics and biopharmaceutics : official journal of Arbeitsgemeinschaft fur Pharmazeutische Verfahrenstechnik e.V*, 2004, **57**, 19-34.
42. R. Chen, X. Cai, K. Ma, Y. Zhou, Y. Wang and T. Jiang, *Biofabrication*, 2017, **9**, 025028.
43. L. Chronopoulou, Y. Toumia, B. Cerroni, D. Pandolfi, G. Paradossi and C. Palocci, *New biotechnology*, 2017, **37**, 138-143.
44. C. Y. Zhang, L. E. Parton, C. P. Ye, S. Krauss, R. Shen, C. T. Lin, J. A. Porco, Jr. and B. B. Lowell, *Cell metabolism*, 2006, **3**, 417-427.
45. K. N. Nam, Y. S. Choi, H. J. Jung, G. H. Park, J. M. Park, S. K. Moon, K. H. Cho, C. Kang, I. Kang, M. S. Oh and E. H. Lee, *International immunopharmacology*, 2010, **10**, 493-499.
46. H. J. Koo, K. H. Lim, H. J. Jung and E. H. Park, *Journal of ethnopharmacology*, 2006, **103**, 496-500.
47. F. Li, W. Li, X. Li, F. Li, L. Zhang, B. Wang, G. Huang, X. Guo, L. Wan, Y. Liu, S. Zhang, S. Kang and J. Ma, *Journal of ethnopharmacology*, 2016, **185**, 77-86.
48. H. J. Koo, Y. S. Song, H. J. Kim, Y. H. Lee, S. M. Hong, S. J. Kim, B. C. Kim, C. Jin, C. J. Lim and E. H. Park, *European journal of pharmacology*, 2004, **495**, 201-208.
49. Y. Koriyama, K. Chiba, M. Yamazaki, H. Suzuki, K. Muramoto and S. Kato, *Journal of neurochemistry*, 2010, **115**, 79-91.
50. S. Habtemariam, *Molecules*, 2018, **23**.
51. S. Habtemariam, *International journal of molecular sciences*, 2017, **19**.
52. B. R. Kim, Y. A. Jeong, Y. J. Na, S. H. Park, M. J. Jo, J. L. Kim, S. Jeong, S. Y. Lee, H. J. Kim, S. C. Oh and D. H. Lee, *Oncotarget*, 2017, **8**, 101952-101964.
53. R. Wang, K. C. MoYung, Y. J. Zhao and K. Poon, *International journal of medical sciences*, 2016, **13**, 507-516.
54. E. S. Kim, C. S. Jeong and A. Moon, *Oncology reports*, 2012, **27**, 567-572.
55. H. Y. Hong and B. C. Kim, *Biochemical and biophysical research communications*, 2007, **362**, 307-312.
56. I. Dando, R. Pacchiana, E. D. Pozza, I. Cataldo, S. Bruno, P. Conti, M. Cordani, A. Grimaldi, G. Butera, M. Caraglia, A. Scarpa, M. Palmieri and M. Donadelli, *Free radical biology & medicine*, 2017, **113**, 176-189.
57. B. C. Kim, H. G. Kim, S. A. Lee, S. Lim, E. H. Park, S. J. Kim and C. J. Lim, *Biochemical pharmacology*, 2005, **70**, 1398-1407.
58. N. Wang, M. Zhu, S. W. Tsao, K. Man, Z. Zhang and Y. Feng, *PloS one*, 2012, **7**, e46318.
59. H. Ko, J. M. Kim, S. J. Kim, S. H. Shim, C. H. Ha and H. I. Chang, *Bioorganic & medicinal chemistry letters*, 2015, **25**, 4191-4196.
60. J. M. Kim, H. Ko, S. J. Kim, S. H. Shim, C. H. Ha and H. I. Chang, *Journal of biochemical and molecular toxicology*, 2016, **30**, 45-54.
61. J. H. Lee, D. U. Lee and C. S. Jeong, *Food and chemical toxicology : an international journal published for the British Industrial Biological Research Association*, 2009, **47**, 1127-1131.
62. O. Chaudhuri, L. Gu, D. Klumpers, M. Darnell, S. A. Bencherif, J. C. Weaver, N. Huebsch, H. P. Lee, E. Lippens, G. N. Duda and D. J. Mooney, *Nature materials*, 2016, **15**, 326-334.
63. A. F. Habeeb, *Analytical biochemistry*, 1966, **14**, 328-336.
64. W. A. Bubnis and C. M. Ofner, 3rd, *Analytical biochemistry*, 1992, **207**, 129-133.
65. Sang-WonLee, J.-M. Lim, S.-H. Bhoo, Y.-S. Paik and T.-R. Hahn, *Analytica Chimica Acta*, 2003, **480**, 267-274.
66. F. Gelain, D. Silva, A. Caprini, F. Taraballi, A. Natalello, O. Villa, K. T. Nam, R. N. Zuckermann, S. M. Doglia and A. Vescovi, *ACS nano*, 2011, **5**, 1845-1859.
67. A. P. Hammersley, *ESRF Internal Report*, 1997.
68. R. Pugliese, F. Fontana, A. Marchini and F. Gelain, *Acta biomaterialia*, 2018, **66**, 258-271.

69. R. L. Horan, K. Antle, A. L. Collette, Y. Wang, J. Huang, J. E. Moreau, V. Volloch, D. L. Kaplan and G. H. Altman, *Biomaterials*, 2005, **26**, 3385-3393.
70. L. Mazzini, M. Gelati, D. C. Profico, G. Sgaravizzi, M. Projetti Pensi, G. Muzi, C. Ricciolini, L. Rota Nodari, S. Carletti, C. Giorgi, C. Spera, F. Domenico, E. Bersano, F. Petruzzelli, C. Cisari, A. Maglione, M. F. Sarnelli, A. Stecco, G. Querin, S. Masiero, R. Cantello, D. Ferrari, C. Zalfa, E. Binda, A. Visioli, D. Trombetta, A. Novelli, B. Torres, L. Bernardini, A. Carriero, P. Prandi, S. Servo, A. Cerino, V. Cima, A. Gaiani, N. Nasuelli, M. Massara, J. Glass, G. Soraru, N. M. Boulis and A. L. Vescovi, *J Transl Med*, 2015, **13**, 17.
71. A. Raspa, G. A. A. Saracino, R. Pugliese, D. Silva, D. Cigognini, A. Vescovi and F. Gelain, *Advanced functional materials*, 2014, **24**, 6317-6328.
72. S. Zhang, *Nat Biotechnol*, 2003, **21**, 1171-1178.
73. F. Taraballi, M. Campione, A. Sassella, A. Vescovi, A. Paleari, W. Hwang and F. Gelain, *Soft Matter*, 2009, **5**, 660-668.
74. E. Genove, C. Shen, S. Zhang and C. E. Semino, *Biomaterials*, 2005, **26**, 3341-3351.
75. F. Taraballi, A. Natalello, M. Campione, O. Villa, S. M. Doglia, A. Paleari and F. Gelain, *Front Neuroeng*, 2010, **3**, 1.
76. A. Horii, X. Wang, F. Gelain and S. Zhang, *PloS one*, 2007, **2**, e190.
77. F. Gelain, S. Panseri, S. Antonini, C. Cunha, M. Donega, J. Lowery, F. Taraballi, G. Cerri, M. Montagna, F. Baldissera and A. Vescovi, *ACS nano*, 2011, **5**, 227-236.
78. M. Alkilzy, R. M. Santamaria, J. Schmoeckel and C. H. Splieth, *Advances in dental research*, 2018, **29**, 42-47.
79. S. Wan, S. Borland, S. M. Richardson, C. L. R. Merry, A. Saiani and J. E. Gough, *Acta biomaterialia*, 2016, **46**, 29-40.
80. M. E. Davis, P. C. Hsieh, T. Takahashi, Q. Song, S. Zhang, R. D. Kamm, A. J. Grodzinsky, P. Anversa and R. T. Lee, *Proceedings of the National Academy of Sciences of the United States of America*, 2006, **103**, 8155-8160.
81. P. C. Hsieh, M. E. Davis, J. Gannon, C. MacGillivray and R. T. Lee, *The Journal of clinical investigation*, 2006, **116**, 237-248.
82. J. H. Jeong, T. G. Park and S. H. Kim, *Pharmaceutical research*, 2011, **28**, 2072-2085.
83. K. Tao, P. Makam, R. Aizen and E. Gazit, *Science*, 2017, **358**.
84. D. E. Discher, D. J. Mooney and P. W. Zandstra, *Science*, 2009, **324**, 1673-1677.
85. G. A. Saracino, D. Cigognini, D. Silva, A. Caprini and F. Gelain, *Chem Soc Rev*, 2013, **42**, 225-262.
86. R. Sarroukh, E. Goormaghtigh, J. M. Ruysschaert and V. Raussens, *Biochimica et biophysica acta*, 2013, **1828**, 2328-2338.
87. M. Sunde, L. C. Serpell, M. Bartlam, P. E. Fraser, M. B. Pepys and C. C. Blake, *J Mol Biol*, 1997, **273**, 729-739.
88. H. Yokoi, T. Kinoshita and S. Zhang, *Proceedings of the National Academy of Sciences of the United States of America*, 2005, **102**, 8414-8419.
89. S. L. Moradi, A. Golchin, Z. Hajishafieeha, M. M. Khani and A. Ardeshirylajimi, *Journal of cellular physiology*, 2018, DOI: 10.1002/jcp.26606.
90. A. F. Martins, S. P. Facchi, P. C. F. da Camara, S. E. A. Camargo, C. H. R. Camargo, K. C. Popat and M. J. Kipper, *Journal of colloid and interface science*, 2018, **525**, 21-30.
91. A. Karimi, S. Karbasi, S. Razavi and E. N. Zargar, *Advanced biomedical research*, 2018, **7**, 44.
92. N. Saadatkish, S. Nouri Khorasani, M. Morshed, A. R. Allafchian, M. H. Beigi, M. Masoudi Rad, R. Esmaeely Neisiany and M. H. Nasr-Esfahani, *Journal of biomedical materials research. Part A*, 2018, DOI: 10.1002/jbm.a.36431.
93. M. Chen, S. Gao, P. Wang, Y. Li, W. Guo, Y. Zhang, M. Wang, T. Xiao, Z. Zhang, X. Zhang, X. Jing, X. Li, S. Liu, Q. Guo and T. Xi, *Journal of biomaterials science. Polymer edition*, 2018, **29**, 461-475.
94. N. H. A. Ngadiman, M. Y. Noordin, A. Idris and D. Kurniawan, *Proceedings of the Institution of Mechanical Engineers. Part H, Journal of engineering in medicine*, 2017, **231**, 597-616.
95. T. G. Kim and T. G. Park, *Tissue engineering*, 2006, **12**, 221-233.
96. J. Yu, A. R. Lee, W. H. Lin, C. W. Lin, Y. K. Wu and W. B. Tsai, *Tissue engineering. Part A*, 2014, **20**, 1896-1907.
97. J. Bockelmann, K. Klinkhammer, A. von Holst, N. Seiler, A. Faissner, G. A. Brook, D. Klee and J. Mey, *Tissue engineering. Part A*, 2011, **17**, 475-486.
98. Seren Hamsici, Goksu Cinar, Asli Celebioglu, Tamer Uyar, A. B. Tekinay and M. O. Guler, *Journal of Materials Chemistry B*, 2017, **5**, 517-524
99. J. R. Paletta, S. Bockelmann, A. Walz, C. Theisen, J. H. Wendorff, A. Greiner, S. Fuchs-Winkelmann and M. D. Schofer, *Journal of materials science. Materials in medicine*, 2010, **21**, 1363-1369.
100. A. S. Tayi, E. T. Pashuck, C. J. Newcomb, M. T. McClendon and S. I. Stupp, *Biomacromolecules*, 2014, **15**, 1323-1327.
101. Surawut Chuangchote, A. Sirivat and P. Supaphol, *Nanotechnology* 2007, **18**.
102. F. Gelain, A. Horii and S. Zhang, *Macromol Biosci*, 2007, **7**, 544-551.
103. C. Cunha, S. Panseri, O. Villa, D. Silva and F. Gelain, *International journal of nanomedicine*, 2011, **6**, 943-955.

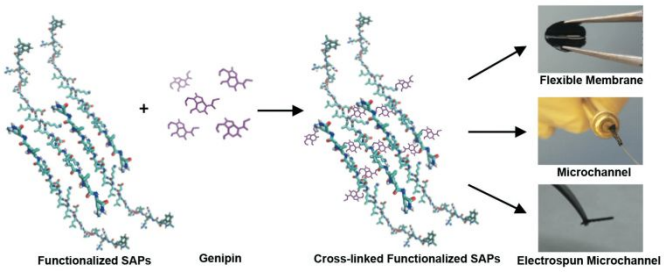

Graphical Abstract

Molecular cross-linking with Genipin enables the production of resilient standard and electro-spun self-standing scaffolds made of self-assembling peptides